ISSN 0915-633X

NATIONAL INSTITUTE FOR FUSION SCIENCE

Analysis of Current Diffusive Ballooning Mode

M. Yagi, K. Itoh, S.-I. Itoh, A Fukuyama and M. Azumi

(Received – Mar. 16, 1993)

NIFS-216 Apr. 1993

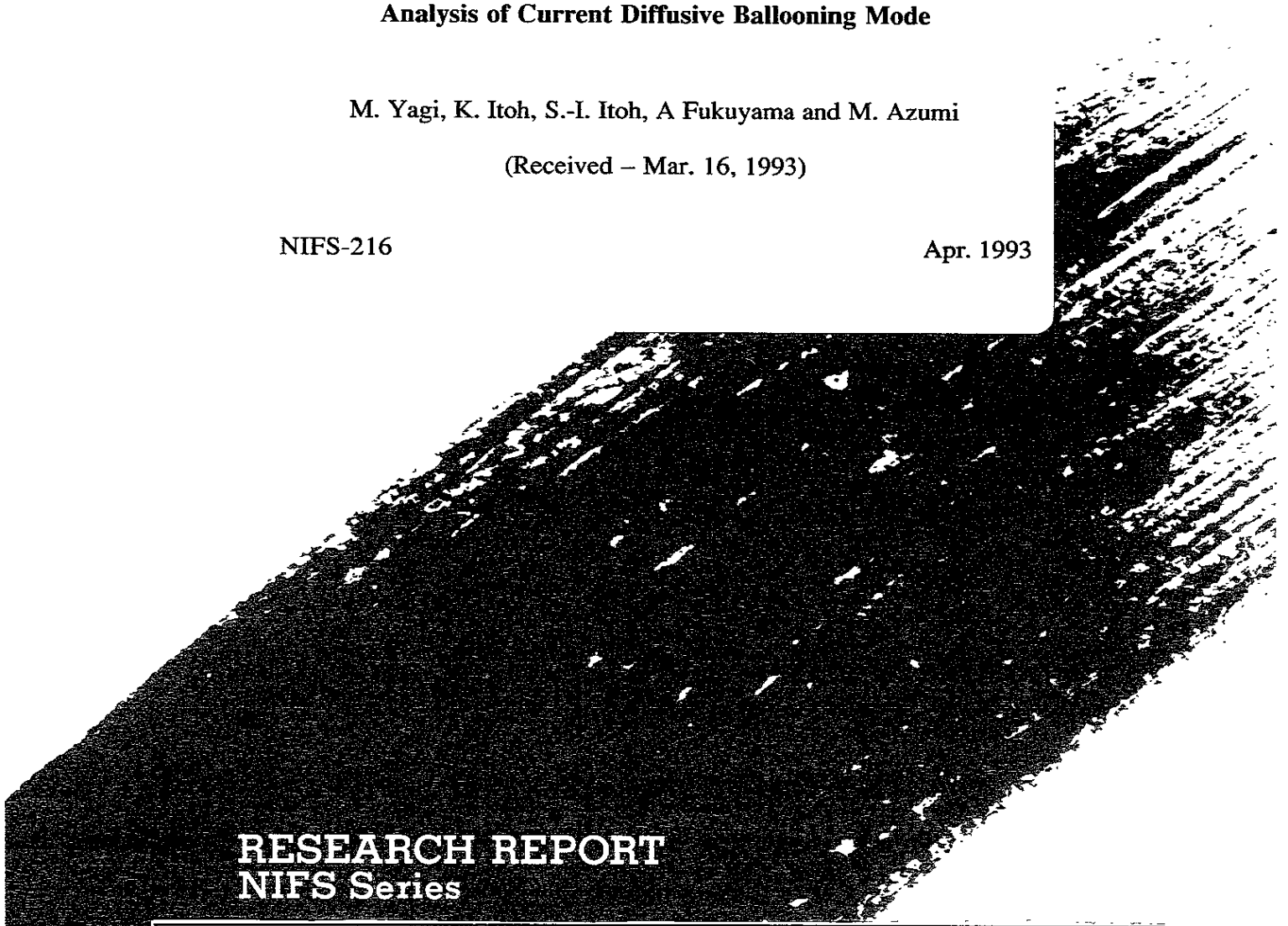

RESEARCH REPORT
NIFS Series

NAGOYA, JAPAN

March 12, 1993

Analysis of Current Diffusive Ballooning Mode

M. Yagi, K. Itoh[†], S.-I. Itoh[††], A. Fukuyama[*] and M.Azumi
Japan Atomic Energy Research Institute
Naka, Ibaraki, 311-01 Japan

[†]National Institute for Fusion Science,
Nagoya 464-01, Japan

[††]Reserch Institute for Applied Mechanics,
Kyushu University 87, Kasuya 816, Japan

[*]Faculty of Engineering, Okayama University,
Okayama 700, Japan

Keywords: Current Diffusivity, Ballooning Mode, L-Mode, Tokamak, Anomalous Transport, Ion Viscosity, Magnetic Shear

The current diffusive ballooning mode is analysed in the tokamak plasma. This mode is destabilized by the current diffusivity (i.e., the electron viscosity) and stabilized by the thermal conductivity and ion viscosity. By use of the ballooning transformation, the eigenmode equation is solved. Analytic solution is obtained by the strong ballooning limit. Numerical calculation is also performed to confirm the analytic theory. The growth rate of the mode and the mode structure are analysed. The stability boundary is derived in terms of the current diffusivity, thermal conductivity, ion viscosity and the pressure gradient for the given shear parameter. This result is applied to express the thermal conductivity in terms of the pressure gradient, magnetic configurational parameters (such as the safety factor, shear and aspect ratio) and the Prandtl numbers.

Index 52.30.-q (52.30.Jb) **52.35.-g** (52.35.Bj, 52.35.Py, 52.35.Ra)

I. Introduction

Ballooning instabilities have been considered to play an important role for the beta limit of tokamak plasma.[1–4] (Beta value is the ratio between the plasma pressure to the magnetic pressure). The stability boundary against the ballooning mode has been calculated based on the ideal magnetohydrodynamics (MHD) equations. This stability boundary was compared to the achieved beta value in experiments, and a correlation between them was recognized. Presently, the modes with the ballooning nature (i.e., the amplitude is larger in the region of the bad magnetic curvature) either with low n-value or high-n value play a key role in limiting the beta value (n is the toroidal mode number).

The ballooning modes can become unstable below the critical beta limit of ideal MHD theory due to the finite dissipation of the plasma. The influence of the resistivity has been widely studied.[5,6] It was found that the ballooning instability persists below the ideal MHD limit of the beta value, and the growth rate is the increasing function of the resistivity. Since the plasma temperature is lower near the egde, this mode can be important near the plasma edge. Theories have been made on the transport driven by the

resistive ballooning mode.[7,8] The theoretical prediction has been given as $\chi \propto (v_e\eta/v_A\sqrt{q})(\beta_p\epsilon^2 L_s/L_p)^{3/2}$, where χ is the thermal conductivity. The parameter dependence leads to $\chi \propto n_e^2 T^{1/2} q^{5/2}$ (n_e is the density, T is the temperature and q is the safety factor), which turns out inappropreate to experimental observations.[9,10]

To understand the anomalous transport in tokamaks, Ohkawa has proposed the model $\chi \propto (c/\omega_{pe})^2 v_e/(qR)$.[11] This formula may explain the two characteristic features of the experimental observations on the anomous transport, i.e., (1) χ has the radial profile such that it is larger near edge, and (2) χ is increasing if the heating power becomes higher (so as the plasma temperature). The essence of the Ohkawa model is that the finite electron inertia has a key role in determining the spatial scale length of the fluctuations. The collisionless skin depth, not the resistive skin depth, is predicted to determine the correlation length. Several authors have reproduced this formula.[12,13] This model, however, has not fully succeeded to explain the parameter dependence of the tokamak confinement. This was partly because the ballooning nature of the mode was not taken into account.

We here present the analysis of the new ballooning mode instability, which

is driven by the current diffusivity below the critical beta limit of the ideal MHD theory. As was pointed out by Ohkawa, the finite electron inertia effect has more important role than the resistivity in present day plasmas. The resistance in the Ohm's law, ηJ, is replaced by $\eta J - \lambda \triangle J$, where η is the resistivity, J is the current density and λ is the current diffusivity. As is seen in this relation, the current diffusive term becomes more important if the current layer width becomes thinner, i.e., less resistive. (The current diffusivity is originated by the electron viscosity, and has been discussed in relation with the global MHD instabilities[14-17] or dynamics of the reversed field pinch plasmas[18-20] or current drive problems.[21]) By use of the ballooning transformation, the eigenmode equation is solved. We obtain the growth rate, mode structure and the stability boundary against the current-diffusive ballooning mode. The stability boundary is expressed in terms of the current diffusivity, thermal conductivity, the ion viscosity μ, and the pressure gradient. This result is also applied to estimate the thermal conductivity. By employing the Prandtl numbers, μ/χ and λ/χ, the form of the thermal conductivity is derived.[22] The anlysis is performed here for the wide range of the geometrical parameters. Analytic theory was developed to obtain the

explicit formula. The numerical computation is also performed, confirming the analytic calculations.

The constitution of this article is as follows. The basic equation and the ballooning transformation are given in §2. The stability analysis is given in §3. The growth by the current diffusivity is discussed in §3*A*, stabilizing effects of γ and μ are shown in §3*B* and the stability criterion is given in §3*C*. Summary and discussion are given in §4.

II. Basic Equations

To construct the model equations, we will start from moment equation. The Ohm's law is written as

$$E_{\|} = \frac{1}{\epsilon n_e} R_{\|}, \tag{1}$$

where $E_{\|}$ is the parallel electric filed, and $R_{\|}$ is the friction force. The frictional force is written taking into account the resistivity and current diffusivity

$$\frac{1}{\epsilon n_e} R_{\|} = \eta J - \lambda \triangle J. \tag{2}$$

The perpendicular ion fluid velocity is given by

$$\boldsymbol{v}_{\perp}^{i} = \frac{\boldsymbol{B}}{B^2} \times \left(-\boldsymbol{E} - \frac{\nabla P_i + \nabla \cdot \Pi_i}{\epsilon n_i} \right). \tag{3}$$

where P_i, the ion pressure, and $\nabla \cdot \Pi_i$, the ion stress tensor due to the ion viscosity. The electron temperature evolution equation is cast into

$$\frac{3}{2} n_e \frac{dT_e}{dt} = -\nabla_\perp \cdot \boldsymbol{q}_{e\perp}, \tag{4}$$

where n_e, the electron density, T_e, the electron temperature, and $\boldsymbol{q}_{e\perp}$, the electron thermal flow by the cross field transport.[29] The cross field transport process is taken into account through the current diffusivity, ion viscosity, μ and thermal transport coefficient, χ. We write,

$$\Pi = -\mu \nabla_\perp \boldsymbol{v}_\perp \tag{5}$$

$$q = -\chi \nabla_\perp p \tag{6}$$

where only the diagonal elements are kept. (λ, μ, χ) can be expressed by turbulent fluctuations. Details will be reported in separate article [23], and in this article we keep (λ, μ, χ) as given parameters. We will briefly discuss the typical values of these terms in Appendix. According to the conventional reduction scheme[24,25](See also Ref.26), we obtain reduced MHD model equations which describe the ballooning modes excited by current diffusive term

as,[18–20,27,28]

$$\frac{n_0 m_i c}{B_0}\left(\frac{\partial}{\partial t}\nabla_\perp^2\phi+\frac{c}{B_0}[\varphi,\nabla_\perp^2\varphi]\right)=\frac{B_0}{c}\nabla_\parallel j_\parallel+\nabla p\times\nabla\frac{2r\cos\theta}{R_0}\hat{z}+\mu m_i n_0\frac{c}{B_0}\nabla_\perp^4\phi \tag{7}$$

$$\frac{1}{c}\frac{\partial A}{\partial t}=-\nabla_\parallel\phi-\eta_\parallel j_\parallel+\lambda\nabla_\perp^2 j_\parallel \tag{8}$$

$$\frac{\partial}{\partial t}p+\frac{c}{B_0}[\phi,p]=\chi_\perp\nabla_\perp^2 p \tag{9}$$

where $j_\parallel=-(c/4\pi)\nabla_\perp^2 A$, ϕ, the electrostatic potential, A, the electromagnetic potential, p, the electron pressure where we assume n_e is constant, and we dropped off the subscript "e" for convenience.

The eigenmode equation is obtained by linearizing Eqs.(7)-(9). This set of partial differential equation is analyzed by the ballooning transformations. When the mode number is high, the mode structure of the ballooning mode is described in the toroidal coordinates (r,θ,ζ) as,

$$\phi(\Delta r,\theta,\zeta)=\sum_{l=-\infty}^{\infty}\hat{\phi}(\theta+2\pi l)\exp[inq'\Delta r(\theta+2\pi l)-imq_0 r_{mn}^{-1}\Delta r\rho\sin\theta+in(q_0\theta-\zeta)], \tag{10}$$

where $\Delta r=r-r_{mn}$, r_{mn} is the radius satisfying $q(r_{mn})=q_0=m/n$, $q'=dq/dr|_{r=r_{mn}}$, $\rho=\sqrt{\beta}q_0^2R_0L_p^{-1}$, $\beta=8\pi P_0/B_0^2$, and $L_p^{-1}=-dlnP_0/dr_{mn}$. We note that θ in Eq.(10) is defined in a covering space,[2,30] $-\infty<\theta<+\infty$,

and a large θ region corresponds to a small Δr region in the ballooning representation of (10). By substituting the ballooning representation into the linearized form of Eqs. (7)-(9), and using the following normalization

$$\begin{aligned} &\frac{t}{\tau_{PA}} \to t, \quad \frac{A}{r_{mn}B_\theta} \to A, \quad \frac{c\tau_{PA}\phi}{B_0 r_{mn}^2} \to \phi, \quad \frac{8\pi p}{B_\theta^2} \to p, \\ &\frac{\tau_{PA}\chi_\perp}{r_{mn}^2} \to \chi, \quad \frac{\tau_{PA}\mu}{n_0 m_i r_{mn}^2} \to \mu, \quad \frac{c^2\eta_\parallel \tau_{PA}}{4\pi r_{mn}^2} \to \eta, \quad \frac{c^2\lambda\tau_{PA}}{4\pi r_{mn}^4} \to \lambda \end{aligned} \tag{11}$$

where $\tau_{PA}^2 = 4\pi n_0 m_i r_{mn}^2/B_\theta^2$, we obtain

$$-n^2q^2f^2\gamma\hat{\phi} = \frac{\partial}{\partial\theta}n^2q^2f^2\hat{A} - inq\epsilon\hat{p}(\bar{\kappa} + \cos\theta + (s\theta - \rho\sin\theta)\sin\theta) + \hat{\mu}n^2q^2f^4\hat{\phi} \tag{12}$$

$$\gamma\hat{A} = -\frac{\partial\hat{\phi}}{\partial\theta} - \hat{\eta}f^2\hat{A} - \hat{\lambda}f^4\hat{A} \tag{13}$$

$$\gamma\hat{p} + inq\frac{\rho}{\epsilon}\hat{\phi} = -\hat{\chi}f^2\hat{p} \tag{14}$$

where γ is the growth rate, $\hat{\eta} = \eta n^2q^2$, $\hat{\lambda} = \lambda n^4q^4$, $\hat{\mu} = \mu n^2q^2$, $\hat{\chi} = \chi n^2q^2$, $\bar{\kappa} = -\epsilon(1 - 1/q^2)$, $\epsilon = r/R_0$, and $f^2 = 1 + (s\theta - \rho\sin\theta)^2$. Combining these equations, we obtain the eigenvalue equation

$$\begin{aligned} f^2\gamma^2\hat{\phi} &= \frac{\partial}{\partial\theta}\frac{f^2}{1 + \frac{\hat{\eta}f^2}{\gamma} + \frac{\hat{\lambda}f^4}{\gamma}}\frac{\partial\hat{\phi}}{\partial\theta} - \gamma\hat{\mu}f^4\hat{\phi} \\ &\quad + \frac{\rho}{1 + \frac{\hat{\chi}f^2}{\gamma}}[\bar{\kappa} + \cos\theta + (s\theta - \rho\sin\theta)\sin\theta]\hat{\phi}. \end{aligned} \tag{15}$$

This equation is solved with the boundary condition that $|\hat{\phi}| \to 0$ as $|\theta| \to \infty$.

III. Stability Analysis

III-A. Destabilization by the current diffusivity

III-A-1. Analytic Estimate

At first, we study the destabilization by the current diffusivity. Eq.(15) is solved by neglecting $\hat{\mu}$ and $\hat{\chi}$. The characteristic inertia scale is given by $\theta \simeq \theta_t = 1/(s\gamma)$ and the current diffusive scale length is given by $\theta \simeq \theta_\lambda = \gamma^{1/4}/(\hat{\lambda}^{1/4}s)$. A self consistent ordering for the growth rate γ is found by equating $\theta_t \simeq \theta_\lambda$ or $\gamma \simeq \lambda^{1/5}(nq)^{4/5}$.

III-A-1-1. Strong Ballooning Limit

We consider the strong ballooning limit in this subsection. Firstly, we search the mode which is localized around $\theta \simeq 0$. In the limit of $1 \ll s$, $\rho \ll s$, $\gamma^{1/2}/(\eta^{1/2}nqs), \gamma^{1/4}/(\lambda^{1/4}nqs), 1/s \ll \theta \ll 1/\sqrt{|s-1/2|}$, $\overline{\kappa} \simeq 0$ which corresponds to the ordering of $1 + \hat{\eta}f^2/\gamma + \hat{\lambda}f^4/\gamma \simeq \hat{\eta}f^2/\gamma + \hat{\lambda}f^4/\gamma$, and $\cos\theta + (s\theta - \rho\sin\theta)\sin\theta \simeq 1$. By using these limiting conditions, the model equation is approximately written by

$$\frac{\partial^2\hat{\phi}}{\partial\theta^2} + \frac{\hat{\eta}}{\gamma}(1 + \frac{\hat{\lambda}}{\hat{\eta}}s^2\theta^2)(\rho - s^2\gamma^2\theta^2)\hat{\phi} \simeq 0 \qquad (16)$$

where we neglected the term proportional to $\partial\phi/\partial\theta$.

Using WKB method, we obtain from Eq.(16)

$$2\sqrt{\frac{\hat{\eta}\rho}{\gamma}}\int_0^{\sqrt{\rho/\gamma^2 s^2}}\sqrt{\left(1-\frac{\gamma^2 s^2}{\rho}\theta^2\right)\left(1+\frac{\hat{\lambda}s^2}{\hat{\eta}}\theta^2\right)}d\theta=\pi\left(l+\frac{1}{2}\right) \tag{17}$$

Integration is performed and the dispersion relation is given by

$$\frac{2}{3}\sqrt{\frac{\hat{\eta}\rho^2}{\gamma^3 s^2}}\sqrt{1+a}\left(\frac{K(k)-E(k)}{k^2}+2E(k)-K(k)\right)=\pi\left(l+\frac{1}{2}\right) \tag{18}$$

where $a=\hat{\lambda}\rho/(\hat{\eta}\gamma^2)$, $k^2=a/(1+a)$. $K(k)$ and $E(k)$ are the first, and second kind of elliptic functions, respectively.

Eq.(18) predicts the resistive ballooning mode and current diffusive ballooning mode. The growth rate of the resistive ballooning mode is given as by taking the limit of $a\ll 1$ or $\hat{\lambda}\rho\ll\hat{\eta}\gamma^2$,

$$\gamma\simeq\frac{\hat{\eta}^{1/3}\rho^{2/3}s^{-2/3}}{(2l+1)^{2/3}}\left(1+\frac{1}{24}\frac{\hat{\lambda}s^{4/3}(2l+1)^{4/3}}{\hat{\eta}^{5/3}\rho^{1/3}}\right). \tag{19}$$

The growth rate which is proportional to $\eta^{1/3}$ is recovered. The cuurent diffusive ballooning mode is given in the other limit $a\gg 1$. The growth rate is written by

$$\gamma\simeq\left(\frac{1}{3\pi}\right)^{2/5}\frac{\hat{\lambda}^{1/5}\rho^{3/5}s^{-2/5}}{(2l+1)^{2/5}}\left(1+\frac{ln1\sqrt{a_0}-1/2}{a_0}\right) \tag{20}$$

where $a_0=(3\pi/4)^{4/5}\hat{\lambda}^{3/5}s^{4/5}(2l+1)^{4/5}/(\hat{\eta}\rho^{1/5})$.

We next study the mode which is localized at $\theta \simeq \theta_j$, $\theta_j \neq 0$. To treat this case, we approximate the Eq.(20) as follows

$$\frac{\partial^2 \hat{\phi}}{\partial \theta^2} + \frac{1 + \frac{\hat{\lambda}}{\gamma} f^4}{f^2} \left(\rho(\cos\theta + s\theta \sin\theta) - \gamma^2 f^2 \right) \hat{\phi} = 0 \tag{21}$$

where we neglect the first derivate of the line-bending term. The term $\cos\theta + s\theta \sin\theta$ makes the local wells at $\theta \neq 0$ so that the localization of the mode is also occurred at these minima of the potential.

Figure 1 shows the function $-(\cos\theta + s\theta \sin\theta)$ versus θ. Here a_j, and b_j are the positions which satisfy the relation $\cos\theta + s\theta \sin\theta = 0$ and θ_j is the minimum point of the function in the region of $[a_j, b_j]$. The equation giving eigenvalue γ^2 is given by[31]

$$\int_{a_j}^{b_j} p d\theta = \pi \left(l + \frac{1}{2} \right) - (-1)^l \exp\left(- \int_{b_j}^{a_{j+1}} |p| d\theta \right) \cos \frac{n\pi}{J+1} \tag{22}$$

where $l = 0, 1, 2, ...,$ $j = 1, 2, ..., J$ and

$$p^2 = \frac{1 + \hat{\lambda}/\gamma f^4}{f^2} (\rho(\cos\theta + s\theta \sin\theta) - \gamma^2 f^2). \tag{23}$$

To treat analytically, we expand the potential near at the point θ_j. Then the integral $\int p d\theta$ is approximated as

$$\int_{a_j}^{b_j} p d\theta \sim \pi \sqrt{\frac{\hat{\lambda}}{\gamma}} s\theta_j F(\theta_j) \sqrt{-\frac{2}{F''(\theta_j)}} \tag{24}$$

where

$$F(\theta_j) = \rho(\cos\theta_j + s\theta_j \sin\theta_j) - \gamma^2 s^2 \theta_j^2 \tag{25}$$

$$F''(\theta_j) = \rho(2s-1)\cos\theta_j - s\rho\theta_j \sin\theta_j - 2\gamma^2 s^2 \tag{26}$$

where θ_j satisfies with the equation.

$$\rho(s-1)\sin\theta_j + s\rho\theta_j \cos\theta_j - 2\gamma^2 s^2 \theta_j = 0. \tag{27}$$

In the case that s is close to unity, Eq.(27) reduces to $\cos\theta_j \simeq 2s\gamma^2/\rho$. Therefore in the limit of $s\gamma^2/\rho \to 0$, Eq.(27) is approximated as $\cos\theta_j \simeq 0$ and $\theta_j \simeq 5\pi/2 + 2\pi j$, $(j = 1, 2....)$. In this limiting case, neglecting the second term in Eq.(22), we obtain $\gamma \propto \hat{\lambda}\rho(s\theta_j)^3(1-\hat{\lambda}^2\rho(s\theta_j)^7)^2$. This formula suggests that γ is governed by the parameter $s\theta_j$, and the growth rate has maximum value $s_0 = s\theta_j$. In other words, the most unstable mode appears at the $j-th$ well, $\theta_j = s_0/s$. When the shear is reduced, higher mode is more unstable.

III-A-1-2. Weak Ballooning Limit

In this subsection, we discuss the weak ballooning limit.[3–5,32] We start from Eqs.(12)-(14) instead of Eq.(15). Introducing the smallness parameter $\delta \ll 1$,

we assume the ordering $\gamma \sim O(\delta)$, $\eta, \lambda \sim O(\delta)$, $s \sim O(\delta)$, and $\partial/\partial\theta = \partial/\partial\theta + s\partial/\partial z$. The variable $z = s\theta$ represents the slowly varying scale length along the filed line. We expand $\hat{\phi} = \hat{\phi}^{(0)}(z) + \delta\hat{\phi}^{(1)}$, $\hat{p} = \hat{p}^{(0)}(z) + \delta\hat{p}^{(1)}$, $\hat{A} = \hat{A}^{(0)} + \delta\hat{A}^{(1)}$. In the leading order

$$\gamma\hat{p}^{(0)} + inq\frac{\rho}{\epsilon}\hat{\phi}^{(0)} = 0, \quad \frac{\partial}{\partial\theta}(n^2q^2f^2\hat{A}^{(0)}) - inq\epsilon\hat{p}^{(0)}(\cos\theta + z\sin\theta) = 0 \quad (28)$$

In next order we obtain solubility conditions for $A^{(1)}$ and $\phi^{(1)}$. The solubility condition gives the relation

$$-\gamma n^2q^2f^2\hat{\phi}^{(0)} = s\frac{\partial}{\partial z}(n^2q^2f^2\langle\hat{A}^{(0)}\rangle) - inq\epsilon\langle\hat{p}^{(1)}(\cos\theta + z\sin\theta)\rangle \quad (29)$$

$$-s\frac{\partial}{\partial z}\hat{\phi}^{(0)} - \hat{\eta}f^2\langle\hat{A}^{(0)}\rangle - \hat{\lambda}f^4\langle\hat{A}^{(0)}\rangle = \gamma\langle\hat{A}^{(0)}\rangle \quad (30)$$

To complete the set of equations we have for $\phi^{(1)}$ and $p^{(1)}$

$$-\frac{\partial\hat{\phi}^{(1)}}{\partial\theta} - \hat{\eta}f^2\hat{A} - \hat{\lambda}f^4\hat{A}^{(0)} = \gamma\hat{A}^{(0)}, \quad \gamma\hat{p}^{(1)} + inq\frac{\rho}{\epsilon}\hat{\phi}^{(1)} = 0 \quad (31)$$

Combining these equations, we obtain

$$s^2\frac{\partial}{\partial z}\frac{f^2}{\gamma + \hat{\eta}f^2 + \hat{\lambda}f^4}\frac{\partial\hat{\phi}}{\partial z} + \frac{\gamma + \hat{\eta}f^2 + \hat{\lambda}f^4}{2}\frac{\rho^2}{\gamma^2}\hat{\phi} - \gamma f^2\hat{\phi} = 0 \quad (32)$$

The fast resistive mode[7,33] was found in the absence of λ. Setting $\hat{\lambda}$ zero, we obtain

$$\gamma = \hat{\eta}^{1/3}\left(\frac{\rho^2}{2}\right)^{1/3}\left(\frac{\rho^2}{2s^2(2l+1)^2} + 1\right)^{1/3} \quad (33)$$

for $\gamma^3 > \hat{\eta}\rho^2/2$. The term $\rho^2/2$ plays the same role as the unfavorable average curvature term (When there is a hill term $\overline{\kappa} > 0$, then this term is replaced by $\overline{\kappa}\rho$). It seems that conventional weak ballooning treatment is not appropriate for λ mode. In the limit $z \gg (\gamma/\hat{\lambda})^{1/4}, \sqrt{2}\gamma/(\hat{\lambda}^{1/2}\rho)$, the solution of Eq.(18) shows oscillatory behavior like $\phi \sim \sin(az^4/4 - 5\pi/16)$ or $\cos(az^4/4 - 5\pi/16)$, where $a^2 = \hat{\lambda}^2\rho^2/(2\gamma^2 s^2)$ since the term $\hat{\lambda}f^4\rho^2/(2\gamma^2)\hat{o}$ has the positive sign compared to the inertia term, $-\gamma f^2\hat{o}$.

III-A-2. Numerical Results

We assure the analytic results by solving the basic equation numerically. The existence of the localized modes are confirmed.

Figure 2.1 shows the shear dependence on the growth rate. For simplicity, we set $\eta = 0$. Parameters are chosen as $\hat{\lambda} = 6.561 \times 10^{-2}$, $\rho = 0.432$, $\overline{\kappa} = -0.11111$, $\epsilon = 0.125$, and $q = 3$. The number 1 corresponds to the fundamental mode($l = 0$) calculated at $\theta \simeq 0$. The lines denoted by the number 2 and 3 correspond to the fundamental modes($l = 0$) which are localized at $\theta = \theta_j$, ($j = 1$ and $j = 2$). The dashed line corresponds to the higher harmonics, $l = 1$ mode. For the fundamental mode, the growth rate

is found to be proportional to $s^{-0.4}$ in the strong shear limit. This result confirms the analytic result in Eq.(20). In the weak shear limit the growth rate is proportional $s^{0.6}$ which is not explained in the frame work of the strong localization limit.

Figure 2.2 shows the eigenmode structure corresponding to the modes 1-4 in Fig.2.1. The fundamental mode has the mode structure of the strong localization. For the higher modes($l = 0, j = 1$ and $l = 0, j = 2$), the mode itself is localized but the peak position of the mode is shifted out. Especially, in the weak shear limit higher modes have larger growth rate than the fundamental one. This tendency is expalined in the previous subsection.

Figure 3 shows $\hat{\lambda}$ dependence of the growth rate for the fundamental mode. The medium and high shear cases are shown ($s = 0.4$,and $s = 1$). The other parameters are same as Fig.2. In the limit $\hat{\lambda} \gg 0.3$, the growth rate is proportional to $\lambda^{0.2}$. This confirms the analytic estimate Eq.(20).

Figure 4 shows ρ dependence of the growth rate for the fundamental mode with $s = 0.4$ and $s = 1$. The parameters are same as Fig.1. In the limit $\rho < 1$, the growth rate for $s = 1$ is proportional to $\rho^{0.6}$ as predicted theoretically. For the medium shear case, $s = 0.4$ to fitting is made as $\gamma \propto \rho^{0.85} (\rho < 0.7)$

which is a little stronger dependence on ρ compared to the theory $\rho^{0.6}$. This is due to the competition between s and ρ in the potential. It is also noted that, in the medium shear case, the growth rate starts to reduce near $\rho \sim 1$. This is discussed latter.

III-B. Stabilization by the Viscosity & Thermal Conduction on λ mode

III-B-1. Analytic Estimate(Strong Ballooning Limit)

Taking the strong ballooning limit as in the previous subsection, we obtain the following equation

$$\frac{\partial^2 \hat{\phi}}{\partial \theta^2} + \frac{\hat{\lambda}}{\hat{\chi}} \rho \hat{\phi} - \hat{\lambda} \hat{\mu} (s\theta)^6 \hat{\phi} - \gamma \hat{\lambda} (s\theta)^4 \hat{\phi} = 0 \tag{34}$$

where the influence of the thermal conductivity and viscosity are kept. Using WKB method, we obtain

$$2 \int_0^{\theta_0} \sqrt{\frac{\hat{\lambda}}{\hat{\chi}} \rho - \hat{\lambda} \hat{\mu} (s\theta)^6 - \gamma \hat{\lambda} (s\theta)^4} d\theta = \pi \left(l + \frac{1}{2} \right) \tag{35}$$

where θ_0 is the kernel of the integrand. In the case of $\hat{\mu} = 0$, the growth rate is given by

$$\gamma = \frac{\hat{\lambda}^2 \rho^3}{\hat{\chi}^3} \frac{1}{s^4} \left(\frac{B(3/2, 1/4)}{\pi (2l+1)} \right)^4 \tag{36}$$

where B is the beta function. In the case of finite $\hat{\mu}$, we treat this term as perturbation for analytic estimation. Then we obtain

$$\gamma = \frac{\hat{\lambda}^2\rho^3}{\hat{\chi}^3}\frac{1}{s^4}\left(\frac{B(3/2,1/4)}{\pi(2l+1)}\right)^4\left[1-3\frac{\hat{\mu}\hat{\chi}^5}{\hat{\lambda}^3\rho^5}s^6\left(\frac{\pi(2l+1)}{B(3/2,1/4)}\right)^6\right] \quad (37)$$

This approximate form of the growth rate is valid in the range $1 \gg \hat{\mu}\hat{\chi}^5 s^6/(\hat{\lambda}^3\rho^5)$. This result shows that the growth rate is reduced by μ and χ.

Next, we discuss the modes which are localized at $\theta \simeq \theta_j$, $\theta_j \neq 0$. According to the same procedure in the previous section, the analytic result is obtained. The potential is written as $p^2 = \hat{\lambda}/\hat{\chi}(\rho(\cos\theta + s\theta\sin\theta) - \hat{\mu}\hat{\chi}(s\theta)^6 - \gamma\hat{\chi}(s\theta)^4)$. (In the limit $s \to 1$, $\hat{\chi}\hat{\mu}s^5\theta_j^4/\rho, \gamma\hat{\chi}s^3\theta_j^2/\rho \ll 1$, we recover the previous result, i.e. $\theta_j = 5\pi/2 + 2j\pi$.) Expanding the potential near θ_j, the dispersion relation is approximately given by

$$\frac{\hat{\lambda}}{\hat{\chi}}\left(\rho s\theta_j - \hat{\mu}\hat{\chi}(s\theta_j)^6 - \gamma\hat{\chi}(s\theta_j)^4\right)^2 = \frac{1}{8}\left(\rho s\theta_j + 12\gamma\hat{\chi}s^4\theta_j^2 + 30\hat{\chi}\hat{\mu}s^6\theta_j^4\right) \quad (38)$$

The growth rate is given by a complicated form but the reduction of the γ is confirmed. We can also estimate the extremum. We see the growth rate is maximum at $\theta_j \simeq (\rho/\hat{\mu}\hat{\chi})^{1/5}/s$. If $\hat{\chi}\hat{\mu}$ is reduced, the higher mode is more unstable.

III-B-2. Numerical Results

Figure 5 shows the $\hat{\chi}$ dependence of the growth rate. The medium shear case, $s = 0.4$ is shown and other parameters are the same as Fig.2 except $\hat{\lambda}$, $\hat{\mu}$, and $\hat{\chi}$. In this case we take $\hat{\lambda} = 6.56 \times 10^{-2}$, and change $\hat{\mu}$ and $\hat{\chi}$ keeping the relation $\hat{\mu} = \hat{\chi}$. We plot fundamental and second modes. For this particular choice of s, the second mode has larger growth rate in the region $\hat{\chi} < 0.01$ as was shown in Fig.2. However, the damping is faster for higher modes than fundamental one in the region $\hat{\chi} > 0.01$.

Figure 6.1 shows the χ dependence of the growth rate in the case that λ, μ, and χ change together. We choose the relation $\lambda = 1 \times 10^{-3}\chi$, and $\hat{\mu} = \hat{\chi}$. In this case, the growth rate shows the different behavior for the small $\hat{\chi}$ limit compared to Fig.5.(In Fig.5, λ is kept constant.) The higher modes($l = 0, j = 1$ and $l = 0, j = 2$) are more unstable in the small $\hat{\chi}$ limit. Figure 6.2 illustrates the profiles of eigen functions. (a), (b) and (c) corresponds to modes 1, 2 and 3 in Fig.6.1, respectively.

Figure 7 shows the ρ dependence of the growth rate for the various values of (λ, μ, χ). (λ, μ, χ) are changed keeping the relation $\lambda = 1 \times 10^{-3}\chi$ and $\hat{\mu} = \hat{\chi}$. The square is the case of the large transport coefficient, $\chi = 1 \times 10^{-5}$,

the triangle, for the medium value, $\chi = 1 \times 10^{-6}$, and the circle, for the small transport coefficient , $\chi = 1 \times 10^{-7}$. The dashed line corresponds to ideal stability limit. For $\chi > 1 \times 10^{-7}$, the second stability zone is disappeared.

III-C. marginal stability analysis

In this section, we discuss the marginal stability condition. The result is applied to estimate transport coefficient. For the analytic estimation, we restrict our discussion in the strong ballooning limit.

III-C-1. Zero-Shear limit

Firstly, we take zero shear limit and set the growth rate zero in Eq.(15). Expand the potential around $\theta = 0$. we obtain the following equation,

$$\frac{\partial^2 \hat{\phi}}{\partial \theta^2} + \frac{\rho \lambda n^2 q^2}{\chi} \left\{ (1 + \overline{\kappa}) - \left(\frac{1}{2} + \rho \right) \theta^2 \right\} \hat{\phi} - \mu \lambda n^6 q^6 \hat{\phi} = 0 \qquad (39)$$

Using the WKB method, we obtain

$$\sqrt{\left(\frac{1}{2} + \rho \right) \frac{\lambda n^2 q^2}{\chi}} \rho = \frac{\lambda n^2 q^2}{\chi} \rho (1 + \overline{\kappa}) - \lambda \mu n^6 q^6 \qquad (40)$$

In the limit $\rho \ll 1$ and $\overline{\kappa} \simeq 0$, we solve this equation for ρ and obtain the stability boundary on ρ in the form as

$$\sqrt{\frac{\rho}{2}} = \frac{1}{4} \sqrt{\frac{\chi}{\lambda}} \frac{1}{nq} + \frac{1}{4} \sqrt{\frac{\chi}{\lambda} \frac{1}{n^2 q^2} + 8 \mu \chi n^4 q^4} \qquad (41)$$

This result shows that the stability boundary, for fixed values of (λ, μ, χ) is increasing both at small-n and large-n limit. Solving the equation, $\partial\rho/\partial n = 0$, we obtain the critical condition for the most unstable mode as

$$\rho_{min} = \frac{25}{32}\left(\frac{32}{5}\right)^{1/3}\frac{\lambda}{\lambda}(\mu\lambda)^{1/3} \tag{42}$$

with mode number.

$$nq = (\frac{5}{32\mu\lambda})^{1/6} \tag{43}$$

Eq.(42) is rewritten as $\lambda \sim 0.57\rho_{min}^{3/2}(\lambda/\lambda)(\lambda/\mu)^{1/2}$ using the Prandtl numbers, (λ/χ) and (μ/λ). As is shown in Ref.[22], if the stationary state is governed by the relation that the most unstable mode is at the marginal stability condition, then the expression for the thermal conductivity is given as

$$\lambda \simeq 0.57\rho^{3/2}\left(\frac{\lambda}{\lambda}\right)\left(\frac{\lambda}{\mu}\right)^{1/2} \tag{44}$$

For the mode which is localized at $\theta \simeq \theta_j$, we can obtain the marginal criterion transforming $\rho \to \rho(s\theta_j)$, $\mu \to \mu(s\theta_j)$. The result is that ρ_{min} is larger by the factor $s\theta_j$ compared to Eq.(42). In other words, the higher mode has a larger stability zone. (The fact that the higher mode is stabilized faster is shown in Fig.6.)

III-C-2. Strong Shear limit

Next we discuss the strong shear case. In this case Eq.(15) with the condition $\gamma = 0$ is approximated by the following equation,

$$\frac{\partial^2 \hat{\phi}}{\partial \theta^2} + \frac{\lambda}{\chi} \rho n^2 q^2 (G_0 - G_1 (s\theta)^2 - G_2 (s\theta)^4 - G_3 (s\theta)^6) \hat{\phi} = 0 \qquad (45)$$

where

$$G_0 = 1 - N^4, \quad G_1 = \frac{1}{2s^2} - \frac{1}{s} + 3N^4,$$

$$G_2 = \frac{1}{6s^3} - \frac{1}{24s^4} + 3N^4, \quad G_3 = \frac{1}{720s^6} - \frac{1}{240s^5} + N^4$$

where $N^4 = \mu \chi n^4 q^4 / \rho$. If we take the ordering $s \sim O(\epsilon^{-1})$ and $O(\epsilon) < N^4 < O(\epsilon^2)$, These coefficients are approximately given by $G_0 \sim 1 - N^4$, $G_1 \sim -1/s + 3N^4$, $G_2 \sim 3N^4$, $G_3 \sim N^4$. For analytic estimation, we neglect G_2 term(i.e., $s\theta > 1$) and investigate two limiting cases that is $G_1 = 0$ and $G_1 \neq 0$ perturbedly. For the first case ($G_0 \neq 0, G_1 = 0$), the WKB solution of Eq.(45) is solved and we obtain the stability boundary,

$$\rho = \left(\frac{\lambda}{\lambda}\right)^{2/3} \left(\frac{\mu}{\lambda}\right)^{1/3} \chi^{2/3} s^{4/3} \left(\frac{3\pi}{2B(3/2, 1/6)}\right)^{4/3} \frac{1}{N^{4/9}(1 - N^4)^{8/9}} \qquad (46)$$

This stability boundary also has the minimum value at a finite mode number. Estimating the minimum value of Eq.(46), the critical condition is given by

$$\rho_{min} = \frac{9}{2^{8/3}} \left(\frac{3\pi}{2B(3/2,1/6)} \right)^{4/3} \left(\frac{\lambda}{\lambda} \right)^{2/3} \left(\frac{\mu}{\chi} \right)^{1/3} \chi^{2/3} s^{4/3} \tag{47}$$

at the mode number

$$N = \frac{1}{\sqrt{3}}. \tag{48}$$

In the second case ($G_0 \neq 0, G_1 \neq 0$), one obtains

$$\rho = \left(\frac{\pi}{4} \right)^{4/3} \left(\frac{\chi}{\lambda} \right)^{2/3} \left(\frac{\mu}{\chi} \right)^{1/3} \chi^{2/3} s^{4/3} \frac{1}{N^{4/9}(1-N^4)^{8/9}(1+a)^{8/3} I^{4/3}} \tag{49}$$

where

$$a = \frac{1}{3} \frac{1/s - 3N^4}{(1-N^4)^{2/3} N^{4/3}}, \quad I = \int_0^1 dy \sqrt{(1-y^2)(y^4+y^2+1/(1+3a\theta_0^2))}, \quad \theta_0^2 = 1+a$$

Using the ordering for s and N^4, a is the order $O(\epsilon^{1/3}) < a < O(\epsilon^{2/3})$ therefore we regard I as constant. In this case, the critical condition is given by

$$\rho_{min} = \left(\frac{\pi}{4} \right)^{4/3} \frac{3^{1/3}}{7^{1/3} I^{4/3}} \left(\frac{\lambda}{\lambda} \right)^{2/3} \left(\frac{\mu}{\chi} \right)^{1/3} \chi^{2/3} s^{5/3} \tag{50}$$

at the mode number

$$N \simeq \frac{7^{3/4}}{3^{3/4} s^{3/4}} \tag{51}$$

Using the similar argument as Eq.(44), we obtain expression of the transport coefficient. For the first case, $(G_0 \neq 0, G_1 = 0)$, Eq.(47) is rewritten as

$$\chi = \frac{16}{27}\left(\frac{2B(3/2,1/6)}{3\pi}\right)^2\left(\frac{\lambda}{\lambda}\right)\left(\frac{\lambda}{\mu}\right)^{1/2}\frac{\rho^{3/2}}{s^2}. \tag{52}$$

In the second case, we obtain the expression for the transport coefficient from Eq.(50) as

$$\lambda = \left(\frac{4I}{\pi}\right)^2\left(\frac{\tau}{3}\right)^{1/2}\rho^{3/2}\left(\frac{\lambda}{\lambda}\right)\left(\frac{\lambda}{\mu}\right)^{1/2}\frac{1}{s^{5/2}} \tag{53}$$

Comparing Eqs.(44),(52), and (53), we can write

$$\lambda \propto \frac{1}{s^\alpha}\rho^{3/2}\left(\frac{\lambda}{\lambda}\right)\left(\frac{\lambda}{\mu}\right)^{1/2} \tag{54}$$

where $\alpha = 0 \sim 2.5$.

III-C-3. Numerical Results

Figure 8 shows numerical results of the growth rate versus n. The parameters are $\lambda = 1 \times 10^{-9}$, $\lambda = \mu = 1 \times 10^{-5}$, $\rho = 0.432$, $\overline{\kappa} = -0.11111$, $q = 3$, and $s = 0.0.1, 0.4, 1.0$. For larger shear, the maximum growth rate is moved to the lower n. The stability boundary appears at the low-n side and high-n side. At these stability boundaries, the eigenmode (with $\gamma = 0$) has the

localized structure. This confirms the analytic study for the existence of the localized marginal stable modes. Figure 9 shows ρ versus n for the marginal stability conditions for the fixed transport coefficients. The parameters are same as Fig.7 and we plot cases of $s = 0.1, 0.4, 1.0$. The stability condition $\rho(n)$ has the minimum value at the intermediate n-value as is predicted by the theory. For larger shear, ρ_{min} is shifted to lower n. This also assures the theoretical prediction.

Figure 10 shows the toroidal mode numbers of the mode, n which gives maximum growth rate and those for the marginal stability, ρ_{min}. The parameters are same as Figs.7 and 8. The toroidal mode number, n which gives maximum growth rate is fitted with $n \propto 1/s^{0.2}$. The toroidal mode number n of the least stable mode, which gives ρ_{min} in the marginal point, are compared in low shear case and finite shear case. In the low shear limit, n approach to constant. In the regime of $0.5 < s < 1$, n is fitted as $n \propto 1/s$ ($n \sim 10/s$ for these parameters).

These formula show that shear dependence on the growth rate and thermal diffusivity are not described with one power law in general sense. (For very low shear case $\chi \propto s^0$, for strong shear, $\chi \propto s^{-2}$).

IV. Conclusion and Discussion

In this paper, we investigated the linear stability of current diffusive ballooning mode (λ mode). For low temperature plasmas, the resistivity drives the ballooning mode but for high temperature plasmas, the current-diffusivity drives modes. The finite electron inertia and the electron viscosity are the origin of the current diffusivity. The geometrical toroidal effect, magnetic shear and q-value, as well as the pressure gradient are investigated. By employing the ballooning formalism, eigenmode equation is solved. The analytic as well as the numerical calculations are made.

Analytic theory is developed to study the parameter dependence of the mode. we notice that $\gamma \propto \lambda^{1/5}$, so that the small amount of λ is enough to give the large growth rate. Instead of the weak ballooning approximation, we develop the theory for the mode which is not localized at $\theta = 0$. By this method we show another estimation of mode which is relevant of arbitrary shear. In the low shear limit higher mode which is trapped in the local potential is more unstable compared to the fundamental mode.

The stabilization by μ and χ is studied. We estimate the viscosity effect on λ mode and obtain $\gamma \propto \hat{\lambda}^2\rho^3/(\hat{\zeta}^3 s^4)$ in the limit $\mu = 0$. Also we show the

second stability region disappeared for the current-diffusivity. We emphasize that the stabilization is possible when both the μ and χ are finite.

We calculate the marginal stability boundary of λ mode and obtained the transport coefficient driven by the least stable mode. The stability boundary is given as $\rho = C(\mu/\chi)^{1/3}(\chi/\lambda)^{2/3}\lambda^{2/3}g(s)$ where C, numerical constant and $g(s)$, some function of shear, for zero shear, $g(s) = const$, for high shear, $g(s) \sim s^{4/3}$. Though the higher mode has large growth rate at small shear, these modes are easily stabilized by μ, χ. Hence the fundamental mode determines the stability boundary.

The formula of the stability boundary is applied to estimate the thermal conductivity at the saturated turbulence.[22] As is shown in a separate article,[23] coefficients (λ, μ, χ) can be expressed in terms of the back-ground turbulence by the renormalization. The Prandtl numbers are weak function of the fluctuation amplitude. The stability boundary Eqs.(42),(47), (50) are rewritten as the formula of the thermal conductivity. We found $\chi \propto \rho^{3/2}(\lambda/\chi)(\chi/\mu)^{1/2}f(s)$ where $f(s)$ is the function of shear. Function $f(s)$, $f(s) \sim const.(s \to 0).s^2$ (large s); is not described with one power law in general. If we use $\lambda/\chi = \mu_0(c^2/\omega_{pe}^2)/r_{mn}^2$, and $\chi/\mu \sim 1$ we can write transport

coefficient explicitly as $\chi \propto f(s)q^2(\beta'/\epsilon)^{3/2}(c^2/\omega_{pe}^2)v_A/R$. Comparing this formula to Ohkawa model[11] which is written as $\chi \propto q^{-1}\beta^{1/2}(c^2/\omega_{pe}^2)v_A/R$, our model shows the favorite q dependence. Also our model accords to Gyro-Bohm type scaling in the global sense. Dimensional dependence is given by $[\chi] = [T]^{1.5}[a]^{-1}[B]^2$. In the local sense, the transport coefficient is increasing at edge region due to $\beta'^{3/2}$. This means conventional global scaling should be modified with such factor when it is used in the transport simulations. We note the form of χ is also confirmed by scale invariance analysis.[34] Typical wave number is given by $k_\perp = nq/r_{mn} \sim \rho^{1/4}(\chi/\mu)^{1/4}/\chi^{1/2}/r_{mn} \sim (c/\omega_{pe})^{-1}f(s)^{-1/2}\rho^{-1/2}$ which is inversely proportional to poloidal gyro-radius. Here we use the Eq.(48). Saturation amplitude is estimated by mixing length theory and given by $\tilde{n}/n \propto f(s)^{1/2}\rho^{1/2}(c/\omega_{pe})/l_p$ which means larger near edge and for high power and low current.

The stability of the λ mode may be affected by the compressibility effect. The effects of compressibility of the resistive ballooning mode is investigated by Hender et al.[35] Thier conclusion is that at high β_p, the pressure convection limit is a good approximation for instabilities with toroidal mode numbers greater than 10. But lower β_p or higher temperatures the effects of compress-

ibilities are crutial. Especially, the perpendicular compression is important for the ballooning modes. Furthermore, we neglect ion diamagnetic effect and $\nabla_{\parallel} q_{\parallel}$ effect in our system. These also stabilize modes. More qualitative investigation is a future work.

ACKNOWLEDGEMENTS

The continuous encouragement of Dr. S. Tamura is gratefully acknowledged. Authors also thank comments by Dr. H. Sanuki.

This work was partially supported by the Grant-in-Aid for Scientific Research of Ministry of Education Japan and collaboration program between universities and JAERI on fusion.

Appendix

We here briefly show the typical values of the ratio λ/μ and μ/χ. To estimate transport coefficient, we only know the ratios λ/χ, and μ/χ. The ratio λ/χ is obtained from quasi-linear estimation. The kinetic equation for electrons in the presence of magnetic stochasticity[27] can be written as

$$\frac{\partial f_e}{\partial t} + \boldsymbol{v}\cdot\nabla f_e + \frac{e}{m_e}(\boldsymbol{E}+\boldsymbol{v}\times\boldsymbol{B})\cdot\nabla_{\boldsymbol{v}} f_e = \frac{\partial}{\partial x}(|v_\parallel| D_M)\frac{\partial f_e}{\partial \epsilon} + C(f_e) \quad \text{(A.1)}$$

where C is a collision operator and D_M indicates the diffusivity of the magnetic field lines in the presence of stochasticity.

Assuming $f = (f_{M\parallel} + \epsilon \hat{f}_\parallel)(f_{M\perp} + \epsilon \hat{f}_\perp)$, the quasi-linear electric field is evaluated by balancing third term in LHS and the first term in RHS in eq.(A.1), multiplying by $-ev_\parallel/|v_\parallel|$ and integrating over the velocity space,

$$E_\parallel^{QL} = -\epsilon \frac{T_e}{\int \epsilon^2 |v_\parallel| f_M d^3v} \frac{\partial}{\partial x} D_M \frac{\partial J_\parallel}{\partial x} = -e\lambda \frac{\partial^2 J_\parallel}{\partial x^2} \quad \text{(A.2)}$$

where $f_M = f_{M\parallel} \times f_{M\perp}$, and $\lambda = (\sqrt{\pi}/2)\mu_0 (c^2/\omega_{pe}^2) v_{T_e} D_M$. The divergence of quasi-linear heat flow is evaluated multiplying $(1/2)m_e v^2$ to Eq.(A.1) and integrating over velocity space.

$$\nabla_\perp \cdot \boldsymbol{q}_{e\perp}^{QL} = -\frac{\partial}{\partial x}\int \frac{1}{2} m_e v^2 |v_\parallel| D_M \frac{\partial f_M}{\partial x} d^3v = -\frac{\partial}{\partial x} \chi_e n_e \frac{\partial T_e}{\partial x} \quad \text{(A.3)}$$

where $\chi_e = (3/\sqrt{\pi})v_{T_e}D_M$. Then we obtain $\lambda/\chi_e = (\pi/6)\mu_0 c^2/\omega_{pe}^2$.

For ion anomalous viscosity, we assume $\beta < 1$, then the Alfven speed is intermediate to the ion and electron thermal velocities, so that ion responds to the electrostatic fluctuations. In that case we can write the ratio of ion anomous viscosity and thermal transport coefficient as[36]

$$\frac{\mu_i}{\chi_i} = \frac{\sum_k \int \frac{d\omega}{2\pi} \left(\frac{\omega}{k_\parallel v_i}\right)^2 \nu_{\boldsymbol{k},\omega}}{\sum_k \int \frac{d\omega}{2\pi} \left(\frac{\omega}{k_\parallel v_i}\right)^4 \nu_{\boldsymbol{k},\omega}} \tag{A.4}$$

where

$$\nu_{\boldsymbol{k},\omega} = \frac{I_{11} Im Z_i}{\sqrt{2T_\parallel/m_i}|k_\parallel|} \tag{A.5}$$

and Z_i, the plasma dispersion function, $T_\parallel$ the parallel ion temperature and I_{11} is defined as

$$\langle E_\theta(\boldsymbol{k},\omega) E_\theta(\boldsymbol{k}',\omega')\rangle = 2\pi\delta_{\boldsymbol{k},\boldsymbol{k}'}\delta(\omega+\omega')I_{11} \tag{A.6}$$

If we assume I_{11} constant for an eigenmode of frequency ω, and $Im Z_i$ has the Gaussian form, the ratio is order unity. Furthermore, if $\chi_e \sim \chi_i$ is retained, we obtain $\mu_i/\chi_e \sim O(1)$.

References

[1]D. Dobrott, D. B. Nelson, J. M. Greene, A. H. Glasser, M. S. Chance, and E. A. Frieman, Phys. Rev. Lett. **39,** 943(1977).

[2]J. W. Connor, R. J. Hastie, and J. B. Taylor, Proc. R. Soc. London, Ser. A. **365,** 1(1979).

[3]D. Lortz, and J. Nuhrenberg,Nucl. Fusion **19,** 1207 (1979).

[4]B. Coppi, A. Ferreira, and J. J. Ramos, Phys. Rev. Lett. **44,** 990(1980).

[5]H. R. Strauss, Phys. Fluids **24,** 2004(1981).

[6]J. W. Connor, R. J. Hastie, and T. J. Martin, Plasma Phys. Cont. Fusion **27,** 1509(1985).

[7]B. A. Carreras, P. H. Diamond, M. Murakami, J. L. Dunlap, J. D. Bell, H. R. Hicks, J. A. Holmes, E. A. Lazarus, V. K. Pare, P. Similon, C. E. Thomas, and R. M. Wieland, Phys. Rev. Lett. **50,** 503(1983).

[8]P. H. Diamond, B. A. Carreras, Comments Plasma Phys. Control Fusion **10** 271(1987).

[9]R. J. Goldstone, Plasma Phys. Control. Fusion **26,** 87(1984).

[10]P. Yushmanov, et al., Nucl. Fusion **30,** 1999(1990).

[11]T. Ohkawa, Phys. Lett. **67A,**35(1978).

[12]B. B. Kadomtsev, and O. P. Pogutse, in Plasma Physics and Controlled Nuclear Fusion Research 1984 (I.A.E.A. London, 1985). Vol.2, 69.

[13]W. Horton, D.-I. Choi, P. N. Yushmanov, and V. V. Parail, Plasma Phys. Control. Fusion **29,** 901(1987).

[14]J. Schmidt, and S. Yosikawa, Phys. Rev. Lett. **26,** 753(1971).

[15]P. J. Kaw, E. J. Valeo, and P. H. Rutherford, Phys. Rev. Lett. **43,** 1398(1979).

[16]A. Y. Aydemir, Phys. Fluids **B 2** 2135(1990).

[17]A. J. Lichtenberg, K. Itoh, S.-I. Itoh, and A. Fukuyama, Nucl. Fusion **31,** 495(1992).

[18]H. R. Strauss, Phys. Fluids **29,** 3668(1986).

[19]A. Bhattacharjee, and E. Hameiri, Phys. Rev. Lett. **57, 206(1986).**

[20]A. A. Boozer, J. Plasma Phys. **35,** 133(1986).

[21]K. Itoh, S.-I. Itoh, and A. Fukuyama, Comments Plasma Phys. Control Fusion **15,** 11(1992).

[22]K. Itoh, S.-I. Itoh, A. Fukuyama, M. Yagi, and M. Azumi, presented at 14th international conference on Plasma Physics and Controlled Nuclear Fusion Research (Würzburg, IAEA, 1992) paper H-2-2 1993.

See also : K. Itoh, M. Yagi, S.-I. Itoh, A. Fukuyama, M. Azumi, Plasma Phys. Control Fusion **35** (1993) in press.

[23]K. Itoh, et al., paper in preparations.

[24]H. R. Strauss, Phys. Fluids **19,** 134(1986).

[25]H. R. Strauss, Phys. Fluids **20,** 1354(1987).

[26]R. D. Hazeltine, and J. D. Meiss, Phys. Rep. **V.121,1-2** 1(1985).

[27]A. B. Rechester, and M. N. Rosenbluth, Phys. Rev. Lett. **40,**38(1978).

[28]G. G. Craddock, Phys. Fluids **B 3,** 316(1991).

[29]S. I. Braginskii, in Review of Plasma Physics, edited by M. A. Leontovich (Consultants Bureau, New Yourk, 1985), Vol.1, p.205.

[30]R. L. Dewar, and A. H. Glasser, Phys. Fluids **26,** 3038(1983).

[31]J. Heading, An Introduction to Phase-Integral Methods (John Wiley & Sonsinc, New York, 1962) p.123.

[32]A. B. Mikhailovskii, and E. I. Yurchenko, Plasma Phys. **24,** 977(1982).

[33]D. Correa-Restrepo. Z. Naturforsch. **37a,** 848(1982).

[34]J. Connor, Plasma Phys. Control Fusion. **35** (1993) in press.

[35]T. C. Hender. B. A. Carreras. W. A. Cooper. J. A. Holmes. P. H. Diamond. and P. L. Similon, Phys. Fluids **27,** 1439(1984).

[36]S.-I. Itoh. Phys. Fluids **B 4,** 796(1992).

Fig.1 The plot of the function $-(\cos\theta + s\theta\sin\theta)$ versus θ. a_1, b_1, a_2 are the positions which satisfy the relation $\cos\theta + s\theta\sin\theta = 0$.

Fig.2.1 Growth rate versus S.

The growth rate for λ_l mode is calculated for the parameters with $\eta = \chi = \mu = 0$, $\hat{\lambda} = 6.561 \times 10^{-1}$, $\rho = 0.132$, $\overline{\kappa} = -0.11111$. The circle corresponds to the fundamental mode($l = 0$), the triangle corresponds to $l = 0, j = 1$ mode, and the diamond corresponds to $l = 0, j = 2$ mode. The dashed line corresponds to $l = 1$ mode.

Fig.2.2 The mode structures corresponding Fig.2.1.

The mode structures are plotted corresponding to Fig.2.1. The fundamental mode (a) is plotted at $s = 1.0$, the $l = 0, j = 1$ mode (c), at $s = 0.4$, the $l = 0, j = 2$ mode (d), at $s = 0.2$. The $l = 1$ mode (b) is plotted at $s = 5.0$.

Fig.3 Growth rate versus $\hat{\lambda}$.

The growth rate for the λ mode corresponding to the fundamental harmonic is calculated for the parameters with $\eta = \chi = \mu = 0$, $\rho = 0.432$, $\overline{\kappa} = -0.11111$, in the case of median shear($s = 0.4$) and high

shear($s = 1.0$), respectively.

Fig.4 Growth rate versus ρ.

The growth rate for λ mode corresponding to the fundamental harmonic is calculated for the parameters with $\eta = \chi = \mu = 0$, $\hat{\lambda} = 6.561 \times 10^{-1}$, $\overline{\kappa} = -0.11111$, in the case of median shear($s = 0.4$) and high shear(($s = 1.0$), respectively.

Fig.5 Growth rate versus $\hat{\chi}$.

The growth rate for λ mode corresponding to fundamental, and $l = 0, j = 1$ mode are calculated for the parameters with $\hat{\lambda} = 6.561 \times 10^{-1}$, $\hat{\mu} = \hat{\chi}$, $\rho = 0.432$, $\overline{\kappa} = -0.11111$, and $s = 0.4$, respectively.

Fig.6.1 Growth rate versus $\hat{\chi}$.

The growth rate for λ mode corresponding to fundamental, $l = 0, j = 1$, and $l = 0, j = 2$ modes are calculated for the parameters with $\lambda = 10^{-3}\chi$, $\mu = \chi$, $\rho = 0.432$, $\overline{\kappa} = -0.11111$, respectively. The circle represents the fundamental, the square, $l = 0, j = 1$ mode, and the diamond, $l = 0, j = 2$ mode, respectively.

Fig.6.2 The mode structures corresponding to Fig.6.1.

The fundamental mode (a) is plotted at $\hat{\chi} = 4.05 \times 10^{-1}$, the $l = 0, j = 1$ mode (b), at $\hat{\chi} = 3.24 \times 10^{-2}$, and the $l = 0, j = 2$ mode (c), at $\hat{\chi} = 1.62 \times 10^{-3}$.

Fig. 7 The growth rate versus ρ.

The growth rate is calculated with $\lambda = 10^{-3}\chi$ and $\mu = \chi$, $s = 1.0$, $\overline{\kappa} = -0.11111$, $n = 30$, and $q = 3$. Here the circle corresponds to the case with $\chi = 10^{-7}$, the triangle, the case with $\chi = 10^{-6}$, and the square, the case with $\chi = 10^{-5}$. The dashed line corresponds to the ideal stability line.

Fig. 8 Growth rate versus n.

The growth rate of λ mode is calculated for the parameters with $\lambda = 10^{-3}\chi$, $\mu = \chi$, $\rho = 0.432$, $\overline{\kappa} = -0.11111$ in the case of the low shear($s = 0.1$), the median shear($s = 0.4$), and the high shear($s = 1.0$), respectively. The triangle represents the case of $s = 0.1$, the circle, $s = 0.4$, and the square, $s = 1.0$.

Fig. 9 ρ versus n.

The ρ for the marginal point is calculated for the parrameters with

$\lambda = 10^{-3}\chi$, $\mu = \chi$, $\rho = 0.432$, $\overline{\kappa} = -0.11111$ in the case of the low shear($s = 0.1$), the median shear($s = 0.4$), and the high shear($s = 1.0$). The square represents the case of $s = 0.1$, the circle, $s = 0.4$, and the triangle, $s = 1.0$.

Fig. 10 n versus s. n determined by ρ_{min} in the marginal point, and n determined by γ_{max} are callculated for the parameters with $\lambda = 10^{-3}\chi$, $\mu = \chi$, $\rho = 0.432$, $\overline{\kappa} = -0.11111$. The circle represents the n determined by ρ_{min}, and the square, the n determined by γ_{max}

Fig.1

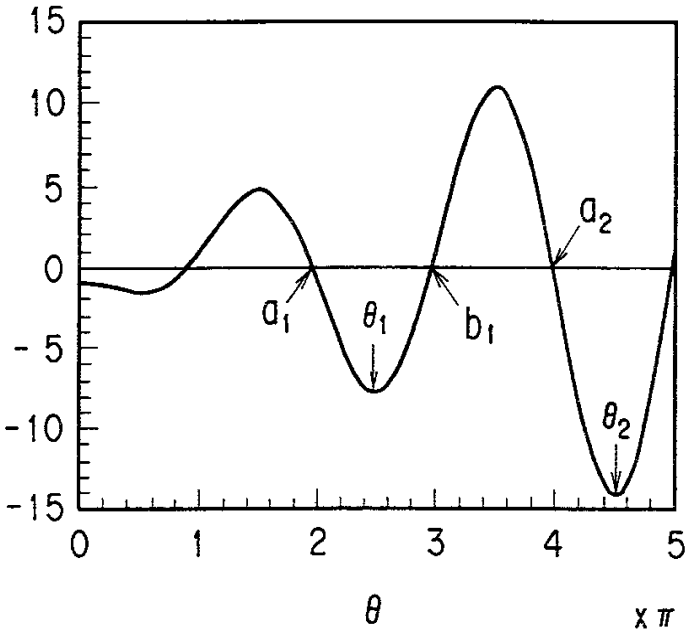

Fig.2.1

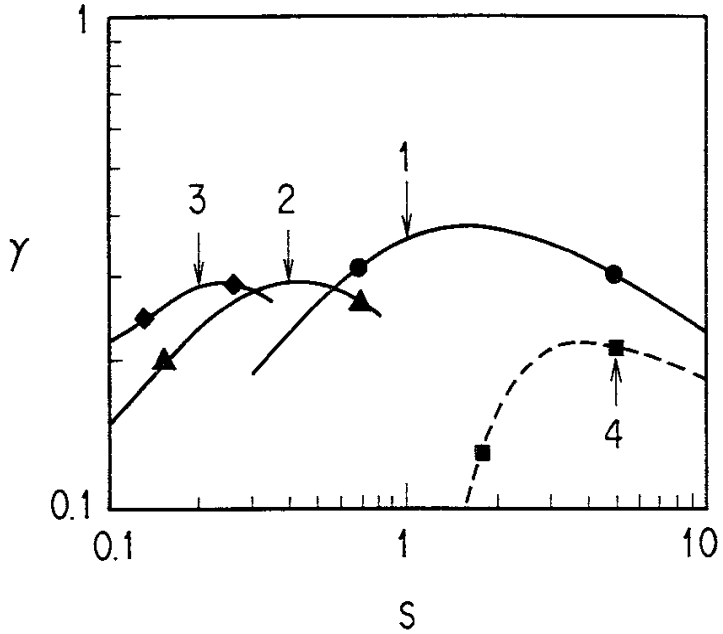

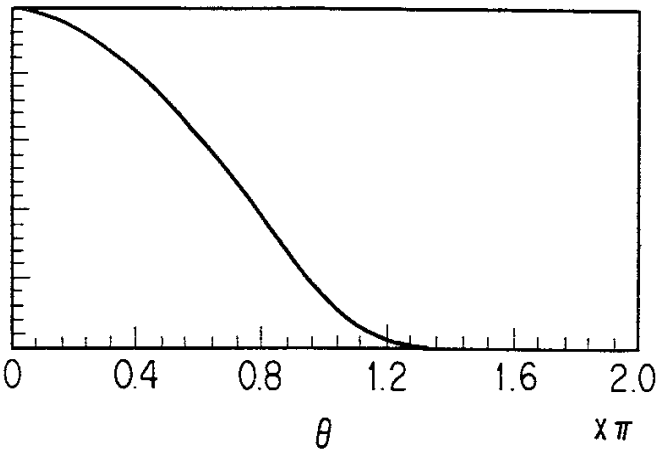
(a)
0
0.4
0.8
1.2
1.6
2.0
θ
x π

Fig.2.2

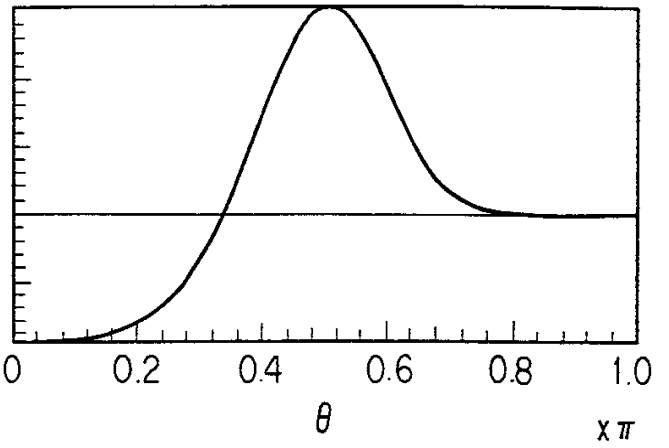
(b)
0
0.2
0.4
0.6
0.8
1.0
θ
x π

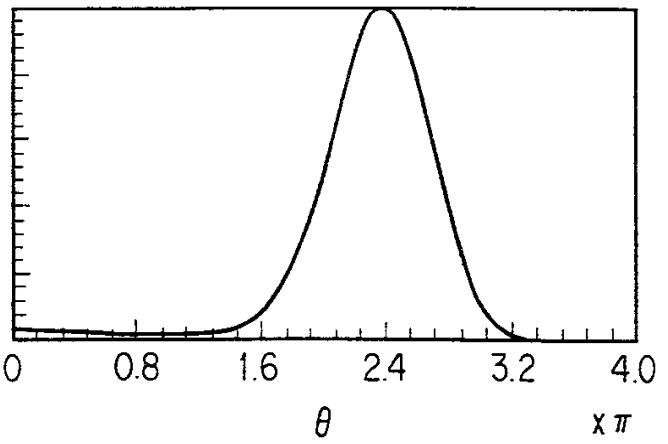
(c)
0
0.8
1.6
2.4
3.2
4.0
θ
x π

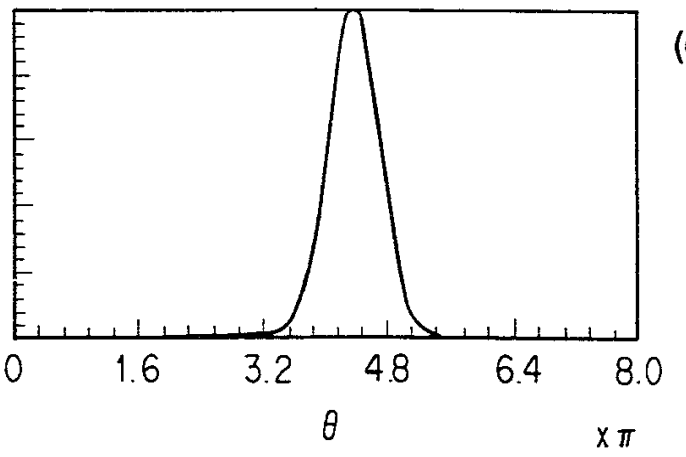
(d)
0
1.6
3.2
4.8
6.4
8.0
θ
x π

Fig.3

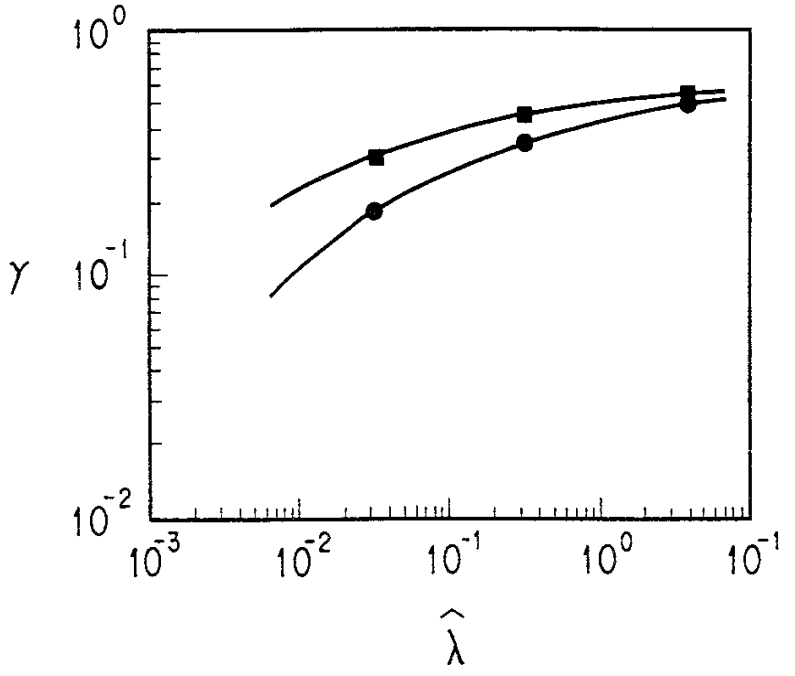
10^0
10^{-1}
10^{-2}
γ
10^{-3}
10^{-2}
10^{-1}
10^0
10^{-1}
$\hat{\lambda}$

Fig.4

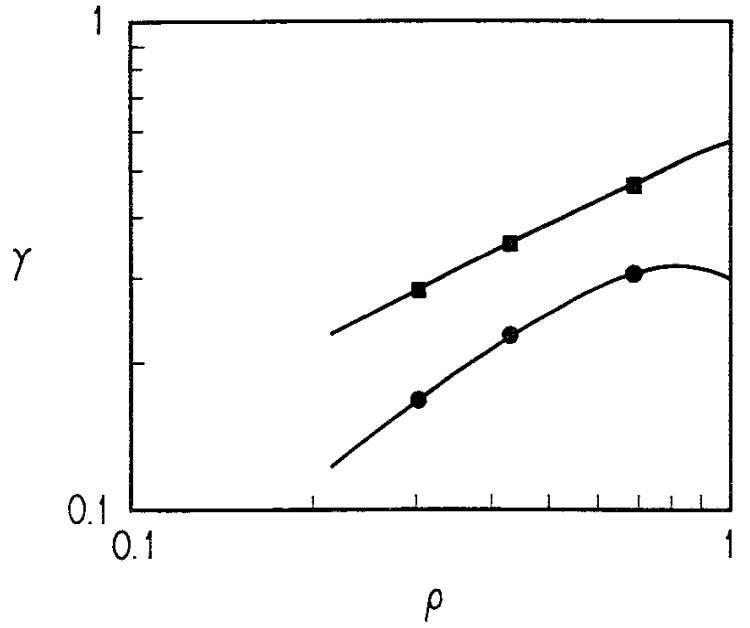
1
0.1
γ
0.1
1
ρ

Fig.5

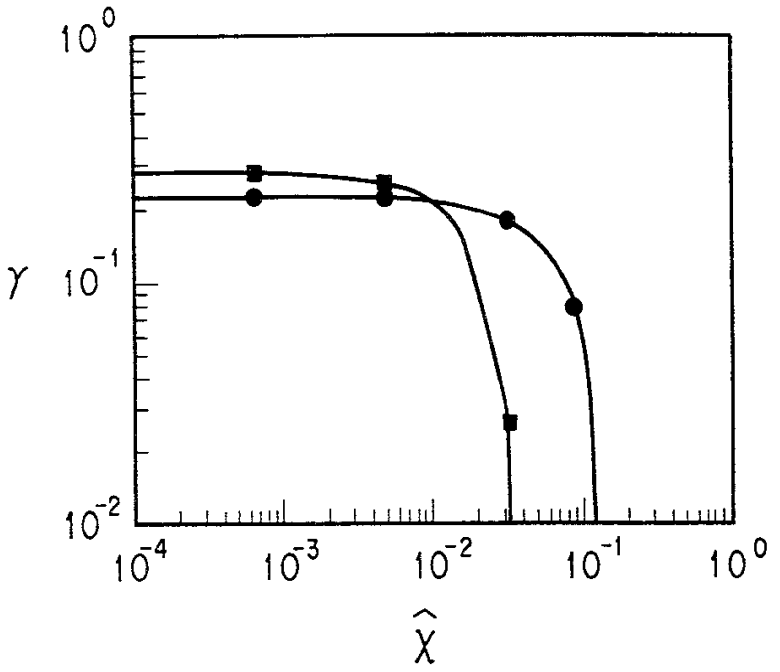
10^0
γ
10^{-1}
10^{-2}
10^{-4}
10^{-3}
10^{-2}
10^{-1}
10^0
$\hat{\chi}$

Fig.6.1

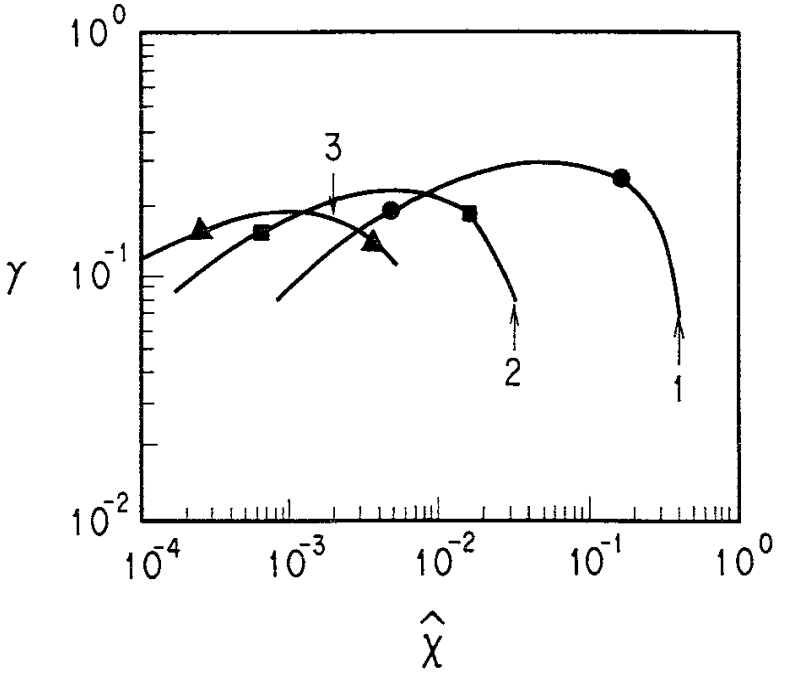
10^0
3
γ
10^{-1}
2
1
10^{-2}
10^{-4}
10^{-3}
10^{-2}
10^{-1}
10^0
$\hat{\chi}$

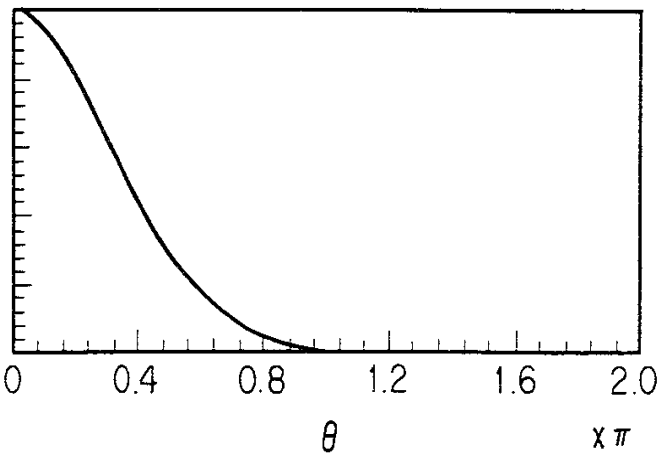

Fig.6.2

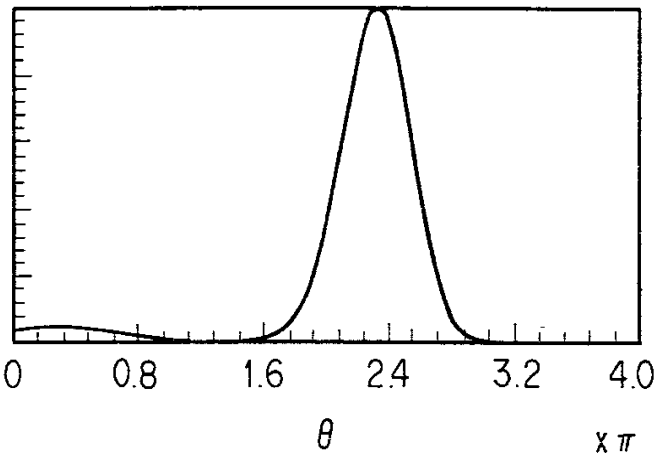

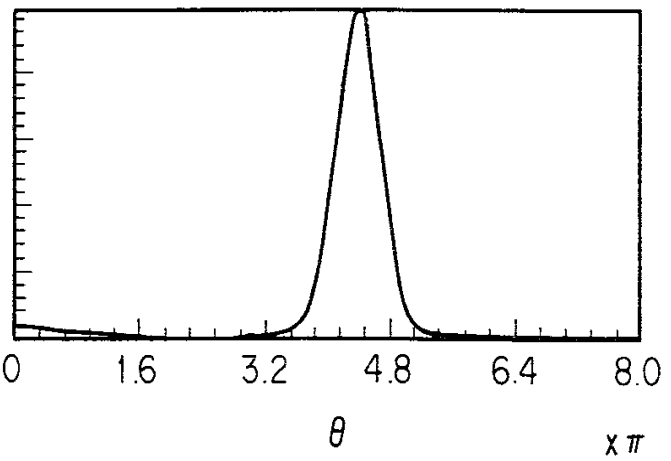

Fig. 7

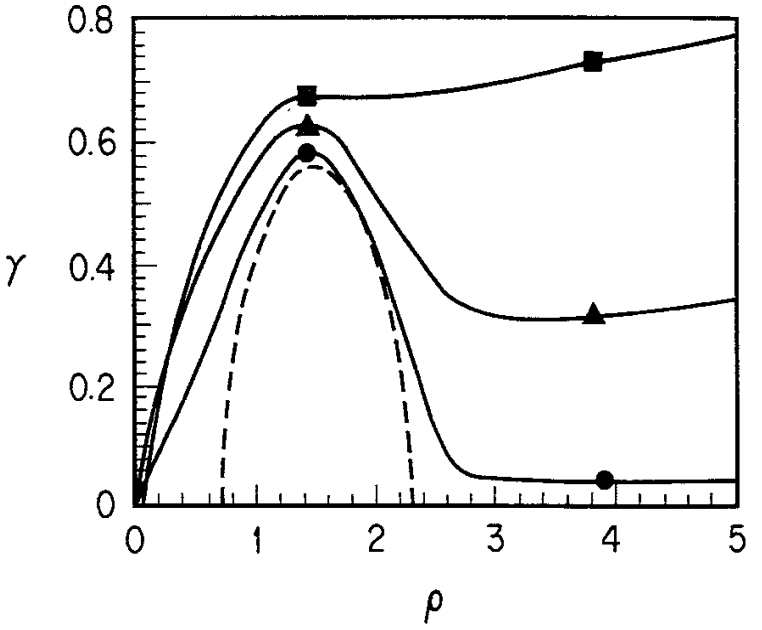

Fig. 8

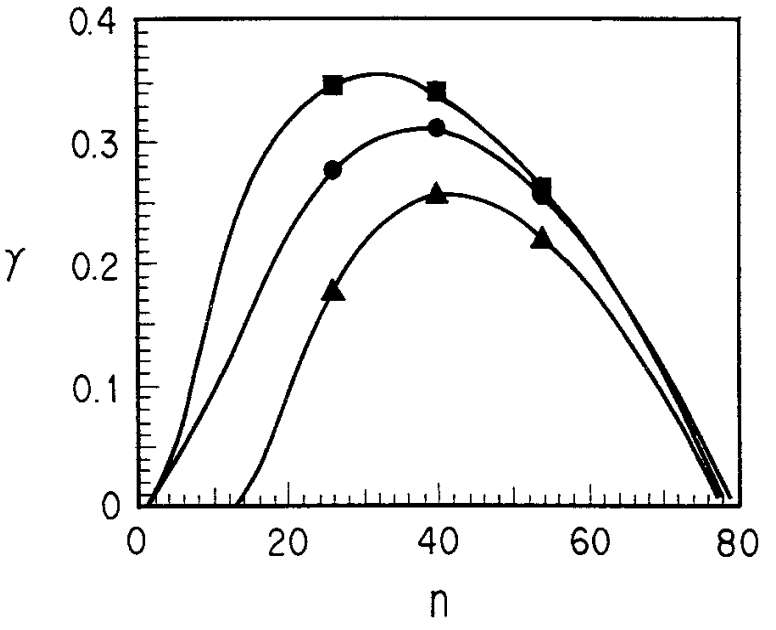

Fig. 9

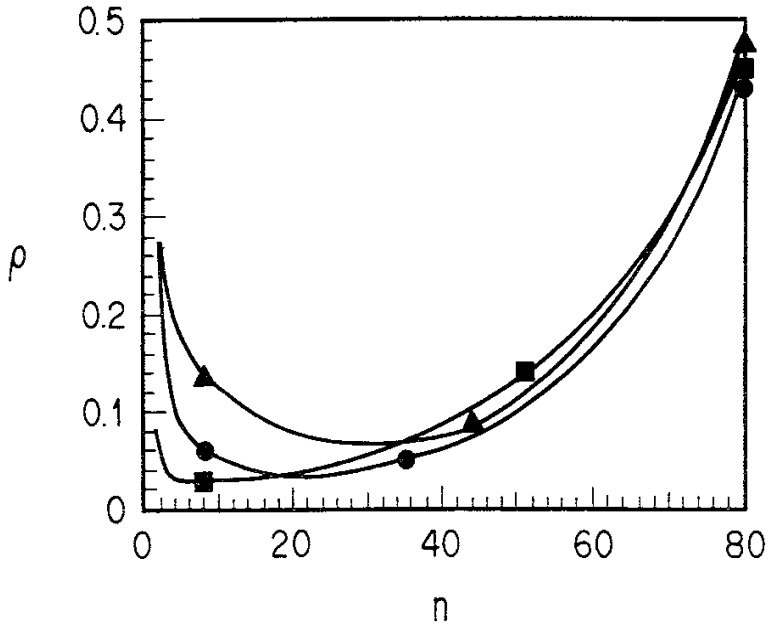

Fig. 10

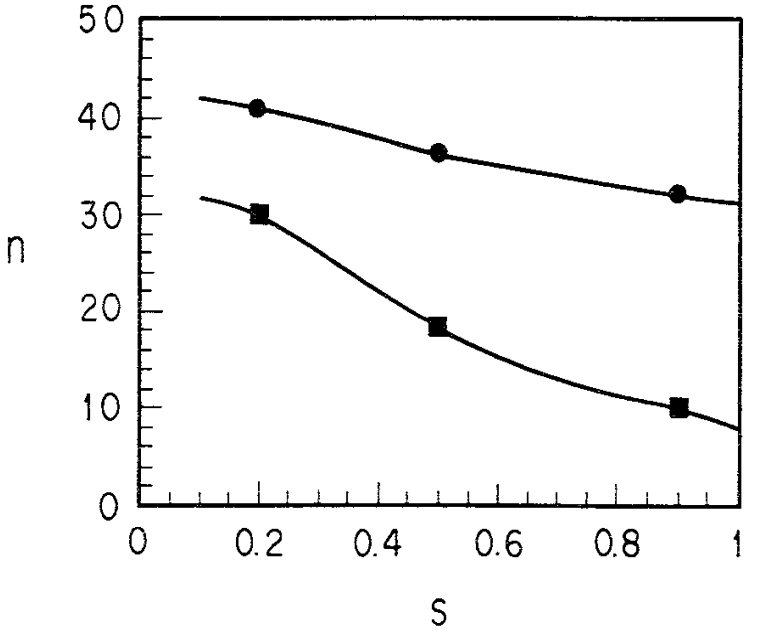

Recent Issues of NIFS Series

NIFS-172 N. Nakajima, M. Okamoto and M. Fujiwara, *Physical Mechanism of E_{ψ}-Driven Current in Asymmetric Toroidal Systems* ; Sep.1992

NIFS-173 N. Nakajima, J. Todoroki and M. Okamoto, *On Relation between Hamada and Boozer Magnetic Coordinate System* ; Sep. 1992

NIFS-174 K. Ichiguchi, N. Nakajima, M. Okamoto, Y. Nakamura and M. Wakatani, *Effects of Net Toroidal Current on Mercier Criterion in the Large Helical Device* ; Sep. 1992

NIFS-175 S. -I. Itoh, K. Itoh and A. Fukuyama, *Modelling of ELMs and Dynamic Responses of the H-Mode* ; Sep. 1992

NIFS-176 K. Itoh, S.-I. Itoh, A. Fukuyama, H. Sanuki, K. Ichiguchi and J. Todoroki, *Improved Models of β-Limit, Anomalous Transport and Radial Electric Field with Loss Cone Loss in Heliotron / Torsatron* ; Sep. 1992

NIFS-177 N. Ohyabu, K. Yamazaki, I. Katanuma, H. Ji, T. Watanabe, K. Watanabe, H. Akao, K. Akaishi, T. Ono, H. Kaneko, T. Kawamura, Y. Kubota, N. Noda, A. Sagara, O. Motojima, M. Fujiwara and A. Iiyoshi, *Design Study of LHD Helical Divertor and High Temperature Divertor Plasma Operation* ; Sep. 1992

NIFS-178 H. Sanuki, K. Itoh and S.-I. Itoh, *Selfconsistent Analysis of Radial Electric Field and Fast Ion Losses in CHS Torsatron / Heliotron* ; Sep. 1992

NIFS-179 K. Toi, S. Morita, K. Kawahata, K. Ida, T. Watari, R. Kumazawa, A. Ando, Y. Oka, K. Ohkubo, Y. Hamada, K. Adati, R. Akiyama, S. Hidekuma, S. Hirokura, O. Kaneko, T. Kawamoto, Y. Kawasumi, M. Kojima, T. Kuroda, K. Masai, K. Narihara, Y. Ogawa, S. Okajima, M. Sakamoto, M. Sasao, K. Sato, K. N. Sato, T. Seki, F. Shimpo, S. Tanahashi, Y. Taniguchi, T. Tsuzuki, *New Features of L-H Transition in Limiter H-Modes of JIPP T-IIU* ; Sep. 1992

NIFS-180 H. Momota, Y. Tomita, A. Ishida, Y. Kohzaki, M. Ohnishi, S. Ohi, Y. Nakao and M. Nishikawa, *D-^{3}He Fueled FRC Reactor "Artemis-L"* ; Sep. 1992

NIFS-181 T. Watari, R. Kumazawa, T. Seki, Y. Yasaka, A. Ando, Y. Oka,O. Kaneko, K. Adati, R. Akiyama, Y. Hamada, S. Hidekuma, S. Hirokura, K. Ida, K. Kawahata, T. Kawamoto, Y. Kawasumi, S. Kitagawa, M. Kojima, T. Kuroda, K. Masai, S. Morita, K. Narihara, Y. Ogawa, K. Ohkubo, S. Okajima, T. Ozaki, M. Sakamoto, M. Sasao, K. Sato, K. N. Sato,

F.Shimpo, H. Takahashi, S. Tanahasi, Y. Taniguchi, K. Toi, T. Tsuzuki and M. Ono, *The New Features of Ion Bernstein Wave Heating in JIPP T-IIU Tokamak* ;Sep, 1992

NIFS-182 K. Itoh, H. Sanuki and S.-I. Itoh, *Effect of Alpha Particles on Radial Electric Field Structure in Torsatron / Heliotron Reactor*; Sep. 1992

NIFS-183 S. Morimoto, M. Sato, H. Yamada, H. Ji, S. Okamura, S. Kubo, O. Motojima, M. Murakami, T. C. Jernigan, T. S. Bigelow, A. C. England, R. S. Isler, J. F. Lyon, C. H. Ma, D. A. Rasmussen, C. R Schaich, J. B. Wilgen and J. L. Yarber, *Long Pulse Discharges Sustained by Second Harmonic Electron Cyclotron Heating Using a 35GH$_Z$ Gyrotron in the Advanced Toroidal Facility*; Sep. 1992

NIFS-184 S. Okamura, K. Hanatani, K. Nishimura, R. Akiyama, T. Amano, H Arimoto, M. Fujiwara, M. Hosokawa, K. Ida, H. Idei, H. Iguchi, O. Kaneko, T. Kawamoto, S Kubo, R. Kumazawa, K. Matsuoka, S. Morita, O. Motojima, T. Mutoh, N. Nakajima, N. Noda, M. Okamoto, T. Ozaki, A. Sagara, S. Sakakibara, H. Sanuki T. Seki, T. Shoji, F. Shimbo, C. Takahashi, Y Takeiri, Y. Takita, K. Toi, K. Tsumori, M Ueda, T Watari H Yamada and I. Yamada, *Heating Experiments Using Neutral Beams with Variable Injection Angle and ICRF Waves in CHS* ; Sep. 1992

NIFS-185 H Yamada, S. Morita, K. Ida, S. Okamura, H. Iguchi, S. Sakakibara, K. Nishimura, R. Akiyama, H. Arimoto, M. Fujiwara, K. Hanatani, S. P. Hirshman, K. Ichiguchi, H. Idei, O. Kaneko, T. Kawamoto, S. Kubo, D. K. Lee, K. Matsuoka, O. Motojima, T. Ozaki, V. D. Pustovitov, A. Sagara, H. Sanuki, T. Shoji, C. Takahashi, Y. Takeiri, Y. Takita, S. Tanahashi, J. Todoroki, K. Toi, K. Tsumori, M. Ueda and I. Yamada, *MHD and Confinement Characteristics in the High-β Regime on the CHS Low-Aspect-Ratio Heliotron / Torsatron* ; Sep. 1992

NIFS-186 S. Morita, H. Yamada, H. Iguchi, K. Adati, R. Akiyama, H. Arimoto, M. Fujiwara, Y. Hamada, K. Ida, H. Idei, O. Kaneko, K. Kawahata, T. Kawamoto, S. Kubo, R. Kumazawa, K. Matsuoka, T. Morisaki, K. Nishimura, S. Okamura, T. Ozaki, T. Seki, M. Sakurai, S, Sakakibara, A. Sagara, C. Takahashi, Y Takeiri, H. Takenaga, Y. Takita, K. Toi, K. Tsumori, K. Uchino, M. Ueda, T. Watari, I. Yamada, *A Role of Neutral Hydrogen in CHS Plasmas with Reheat and Collapse and Comparison with JIPP T-IIU Tokamak Plasmas* ; Sep. 1992

NIFS-187 K. Ioth, S.-I. Itoh, A. Fukuyama, M. Yagi and M. Azumi, *Model of the L-Mode Confinement in Tokamaks* ; Sep. 1992

NIFS-188 K. Itoh, A. Fukuyama and S.-I. Itoh, *Beta-Limiting Phenomena in High-Aspect-Ratio Toroidal Helical Plasmas*; Oct. 1992

NIFS-189 K. Itoh, S. -I. Itoh and A. Fukuyama, *Cross Field Ion Motion at Sawtooth Crash* ; Oct. 1992

NIFS-190 N. Noda, Y. Kubota, A. Sagara, N. Ohyabu, K. Akaishi, H. Ji, O. Motojima, M. Hashiba, I. Fujita, T. Hino, T. Yamashina, T. Matsuda, T. Sogabe, T. Matsumoto, K. Kuroda, S. Yamazaki, H. Ise, J. Adachi and T. Suzuki, *Design Study on Divertor Plates of Large Helical Device (LHD)* ; Oct. 1992

NIFS-191 Y. Kondoh, Y. Hosaka and K. Ishii, *Kernel Optimum Nearly-Analytical Discretization (KOND) Algorithm Applied to Parabolic and Hyperbolic Equations* : Oct. 1992

NIFS-192 K. Itoh, M. Yagi, S.-I. Itoh, A. Fukuyama and M. Azumi, *L-Mode Confinement Model Based on Transport-MHD Theory in Tokamaks* ; Oct. 1992

NIFS-193 T. Watari, *Review of Japanese Results on Heating and Current Drive* ; Oct. 1992

NIFS-194 Y. Kondoh, *Eigenfunction for Dissipative Dynamics Operator and Attractor of Dissipative Structure* ; Oct. 1992

NIFS-195 T. Watanabe, H. Oya, K. Watanabe and T. Sato, *Comprehensive Simulation Study on Local and Global Development of Auroral Arcs and Field-Aligned Potentials* ; Oct. 1992

NIFS-196 T. Mori, K. Akaishi, Y. Kubota, O. Motojima, M. Mushiaki, Y. Funato and Y. Hanaoka, *Pumping Experiment of Water on B and LaB_6 Films with Electron Beam Evaporator* ; Oct., 1992

NIFS-197 T. Kato and K. Masai, *X-ray Spectra from Hinotori Satellite and Suprathermal Electrons* ; Oct. 1992

NIFS-198 K. Toi, S. Okamura, H. Iguchi, H. Yamada, S. Morita, S. Sakakibara, K. Ida, K. Nishimura, K. Matsuoka, R. Akiyama, H. Arimoto, M. Fujiwara, M. Hosokawa, H. Idei, O. Kaneko, S. Kubo, A. Sagara, C. Takahashi, Y. Takeiri, Y. Takita, K. Tsumori, I. Yamada and H. Zushi, *Formation of H-mode Like Transport Barrier in the CHS Heliotron / Torsatron* ; Oct. 1992

NIFS-199 M. Tanaka, *A Kinetic Simulation of Low-Frequency Electromagnetic Phenomena in Inhomogeneous Plasmas of Three-Dimensions* ; Nov. 1992

NIFS-200 K. Itoh, S.-I. Itoh, H. Sanuki and A. Fukuyama, *Roles of Electric Field on Toroidal Magnetic Confinement*, Nov. 1992

NIFS-201 G. Gnudi and T. Hatori, *Hamiltonian for the Toroidal Helical Magnetic Field Lines in the Vacuum*; Nov. 1992

NIFS-202 K. Itoh, S.-I. Itoh and A. Fukuyama, *Physics of Transport Phenomena in Magnetic Confinement Plasmas*; Dec. 1992

NIFS-203 Y. Hamada, Y. Kawasumi, H. Iguchi, A. Fujisawa, Y. Abe and M. Takahashi, *Mesh Effect in a Parallel Plate Analyzer*; Dec. 1992

NIFS-204 T. Okada and H. Tazawa, *Two-Stream Instability for a Light Ion Beam -Plasma System with External Magnetic Field;* Dec. 1992

NIFS-205 M. Osakabe, S. Itoh, Y. Gotoh, M. Sasao and J. Fujita, *A Compact Neutron Counter Telescope with Thick Radiator (Cotetra) for Fusion Experiment*; Jan. 1993

NIFS-206 T. Yabe and F. Xiao, *Tracking Sharp Interface of Two Fluids by the CIP (Cubic-Interpolated Propagation) Scheme*, Jan. 1993

NIFS-207 A. Kageyama, K. Watanabe and T. Sato, *Simulation Study of MHD Dynamo : Convection in a Rotating Spherical Shell*; Feb. 1993

NIFS-208 M. Okamoto and S. Murakami, *Plasma Heating in Toroidal Systems*; Feb. 1993

NIFS-209 K. Masai, *Density Dependence of Line Intensities and Application to Plasma Diagnostics*; Feb. 1993

NIFS-210 K. Ohkubo, M. Hosokawa, S. Kubo, M. Sato, Y. Takita and T. Kuroda, *R&D of Transmission Lines for ECH System* ; Feb. 1993

NIFS-211 A. A. Shishkin, K. Y. Watanabe, K. Yamazaki, O. Motojima, D. L. Grekov, M. S. Smirnova and A. V. Zolotukhin, *Some Features of Particle Orbit Behavior in LHD Configurations*; Mar. 1993

NIFS-212 Y. Kondoh, Y. Hosaka and J.-L. Liang, *Demonstration for Novel Self-organization Theory by Three-Dimensional Magnetohydrodynamic Simulation*; Mar. 1993

NIFS-213 K. Itoh, H. Sanuki and S.-I. Itoh, *Thermal and Electric Oscillation Driven by Orbit Loss in Helical Systems*; Mar. 1993

NIFS-214 T. Yamagishi, *Effect of Continuous Eigenvalue Spectrum on Plasma Transport in Toroidal Systems*; Mar. 1993

NIFS-215 K. Ida, K. Itoh, S.-I.Itoh, Y. Miura, JFT-2M Group and A. Fukuyama, *Thickness of the Layer of Strong Radial Electric Field in JFT-2M H-mode Plasmas*; Apr. 1993